Screening Cellulose Spinning Parameters for Fabrication of Novel Carbon Hollow Fiber Membranes for Gas Separation

Linfeng Lei, Arne Lindbråthen, Magne Hillestad, marius Sandru, Evangelos P Favvas, and Xuezhong He

Just Accepted

1
2
3
4
5
6
7
8
9
10
11
12
13
14
15
16
17
18
19
20
21
22
23
24
25
26
27
28
29
30
31
32
33
34
35
36
37
38
39
40
41
42
43
44
45
46
47
48
49
50
51
52
53
54
55
56
57
58
59
60

Screening Cellulose Spinning Parameters for Fabrication of Novel Carbon Hollow Fiber Membranes for Gas Separation

Linfeng Lei[a], Arne Lindbråthen[a], Magne Hillestad[a],*, Marius Sandru[b], Evangelos Favvas[c], Xuezhong He[a],*

[a] Department of Chemical Engineering, Norwegian University of Science and Technology, NO-7491 Trondheim, Norway

[b] SINTEF Industry, SINTEF AS, NO-7465 Trondheim, Norway

[c] Institute of Nanoscience and Nanotechnology, National Center for Scientific Research "*Demokritos*", Aghia Paraskevi 153 41, Athens Greece

*Correspondence: magne.hillestad@ntnu.no (MH); xuezhong.he@ntnu.no (XH), Tel.: +47-7359-3942

1

Abstract

Novel carbon hollow fiber membranes (CHFMs) have been, for the first time, prepared from cellulose precursors directly spun with a cellulose/(1-ethyl-3-methylimidazolium acetate (EmimAc) + dimethyl sulfoxide (DMSO)) system. The spinning parameters such as air gap, dope and bore flow, bore fluid composition and take-up speed are investigated by factorial design method to screen hollow fiber precursors. All the precursors were carbonized using the same controlled protocol, and the prepared CHFMs show good performance that are above the Robeson upper bound of CO_2/CH_4 and O_2/N_2. The best obtained CHFMs shows a CO_2 permeability of 239 Barrer and a CO_2/CH_4 selectivity of 186 from single gas permeation measurement. The CHFM shows attractive CO_2/CH_4 selectivities of 75 and 50 from 10% CO_2/90% CH_4 permeation tests at 25 °C with a feed pressure 28 bar, and 60 °C with 8 bar, respectively. Thus, the developed cellulose-based CHFMs shows potential for gas separation.

Keyword: carbon hollow fiber membranes; cellulose; ionic liquid; spinning; gas separation

2

1. Introduction

Membrane systems are expected to be applied in different gas separations such as oxygen recovery from air [1], natural gas sweetening [2-4] and CO_2 capture from flue gas [5, 6], due to its small footprint, low energy consumption, low capital and operating cost and process flexibility. In the past decades, a few polymeric membranes have been commercialized for industrial gas separations, such as cellulose acetate, polyimide and perfluoro polymer membranes for CO_2 removal from natural gas [2]. However, polymeric membranes application is limited due to membrane compaction and plasticization when applied in high-pressure processes [3], which results in relatively poor separation performances. Moreover, polymeric membranes are subject of an "upper bound" limitation with a trade-off between gas permeability and selectivity [7]. Inorganic membrane materials, like carbon molecular sieving (CMS) membranes [8-13] and zeolite membranes [14, 15], show attractive gas separation performance operated under harsh conditions such as high pressures and high temperatures. Among them, CMS membranes with an ultra-microporous structure are usually prepared by carbonization of polymeric precursors, such as polyimides [8, 10, 16, 17] and cellulose derivatives [5, 18-20]. The ultraselective CMS membranes made from polyimide precursors, showing a potential application on some ultrafine discrimination of closely sized molecules required conditions [10], but the polyimide materials are usually highly cost, which presents a high carbon membrane production cost. Cellulose acetate derived CMS membranes showed good performance on CO_2/CH_4 and CO_2/N_2 separation processes by He et al. [11, 18], and a pilot-scale system was reported to produce CHFMs with an annual production capacity 700 m² from regenerated cellulose precursor [21]. However, the preparation of cellulose acetate derived carbon membranes is challenging due to the difficulties in controlling the drying process for the deacetylated hollow fibers. Thus, spinning of cellulose hollow fibers from a cellulose dope solution directly and then fabrication of CHFMs by a carbonization protocol could be a potential solution to address the challenges. Moreover, cellulose is also a cheap, inexhaustible and bio-renewable material [22-26], which provides a low-cost production progress for making carbon membranes. Ionic liquids (ILs) have been identified as good solvents for cellulose dissolution due to the excellent solubility and unique physicochemical properties,

3

such as low volatility, high thermal and chemical stability[23, 27]. Besides, several IL recycling methods have been investigated involving freeze crystallization [28], membrane separation [29] and evaporation [30]. Thus, development of cellulosic membranes from ILs could be a potential way for the chemical production industry. Our previous work has proved that a cellulose/(1-Ethyl-3-methylimidazolium acetate (EmimAc) + dimethyl sulfoxide (DMSO)/H_2O ternary system was able to spin defect-free cellulose hollow fibers [31]. Since the precursor properties will influence carbon membrane performance, it is important to investigate cellulose precursor by systematic investigation of spinning parameters (especially for the novel cellulose/ILs spinning system) to identify the proper precursor for making advanced carbon membranes. Various experimental design methods have been reported for preparation of membranes in the literature [32-34] to screen the effect factors during the membrane fabrication process and then optimize the membrane separation performances. For instance, Saljoughi et al. employed a Taguchi experimental design to conduct a minimum number of experiments and identify the contribution of factors in an asymmetric cellulose acetate membranes synthesis process [35]. Khayet et al. used a fractional factorial design to investigate the combined effects of polymer and additive content in casting solutions, evaporation time of solvent and coagulation temperature on the structures and performance of prepared membranes [34].

In this work, novel carbon hollow fiber membranes (CHFMs) are prepared based on cellulose hollow fiber precursors spun from cellulose/ionic liquids system. DMSO was added to the solvent to decrease the viscosity of dope solution and reduce the material cost. In order to investigate the effect of precursor on the CMS dimension (thickness, outer diameter) and separation performances (CO_2 permeability and CO_2/CH_4 selectivity), the spinning parameters such as air gap, dope flow, bore flow, bore fluid composition and take-up speed are investigated by experimental design method. The single gas permeation tests and scanning electron microscope (SEM) characterization for all prepared carbon membranes were performed. Further structure and performance characterization on the selected best CHFMs were also conducted by gas adsorption and mixed gas permeation measurements.

4

2. Experimental

2.1 Materials

Microcrystalline cellulose (MCC, Avicel PH-101), glycerol (>99 %, Food Chemicals Codex (FCC) grade) and DMSO (≥99%, FCC grade) used in this work were purchased from Sigma-Aldrich. The ionic liquid of EmimAc was provided by the Institute of Process Engineering, Chinese Academy of Sciences (IPE-CAS). The EmimAc was purified by ethyl acetate before using, and the product purity was confirmed by ^{1}H and[13]C NMR [36]. Tap water was used as the non-solvent in the coagulation and rinsing baths.

2.2 Spinning cellulose hollow fiber precursors

A well-known dry-wet spinning method is employed to fabricate cellulose hollow fibers as is illustrated in **Figure 1a**. A 12 wt.% MCC dope solution was made by dissolving a given amount of MCC in the co-solvent (75 wt.% EmimAc and 25 wt.% DMSO) with mechanical stirring at 50 °C in a glove box (relative humidity of < 1 %) to minimize any contamination from moisture. The spinneret size used for spinning is 0.7 mm/0.5 mm (OD/ID). Before starting the spinning process, filtration and degassing steps were implemented to avoid air bubbles and undissolved cellulose which could lead to macrovoids formation inside hollow fibers. During the spinning process, the temperature of dope solution was kept at 50 °C whereas bore solution, coagulation baths were kept at room temperature. The fabricated cellulose hollow fibers were then placed in a tap-water bath for 24 h to remove excess solvents, and subsequently immersed in a 10% glycerol aqueous solution. Using glycerol aqueous solution before drying hollow fiber membranes can prevent the collapse of porous structures due to a lower vapor pressure compared to water as reported in the literature [37, 38], and is beneficial to reduce the curl formation of cellulose hollow fibers during the drying process. **Figure 1b** shows the cellulose hollow fiber precursors after the treatment with glycerol aqueous solution. The obtained cellulose hollow fibers were finally dried at room temperature for characterization and fabrication of CMS membranes. It should be noted that ionic liquids will be recycled

5

in a large-scale production process to achieve a low environmental impact and reduce the production cost-

this has, however, not been investigated in the current work.
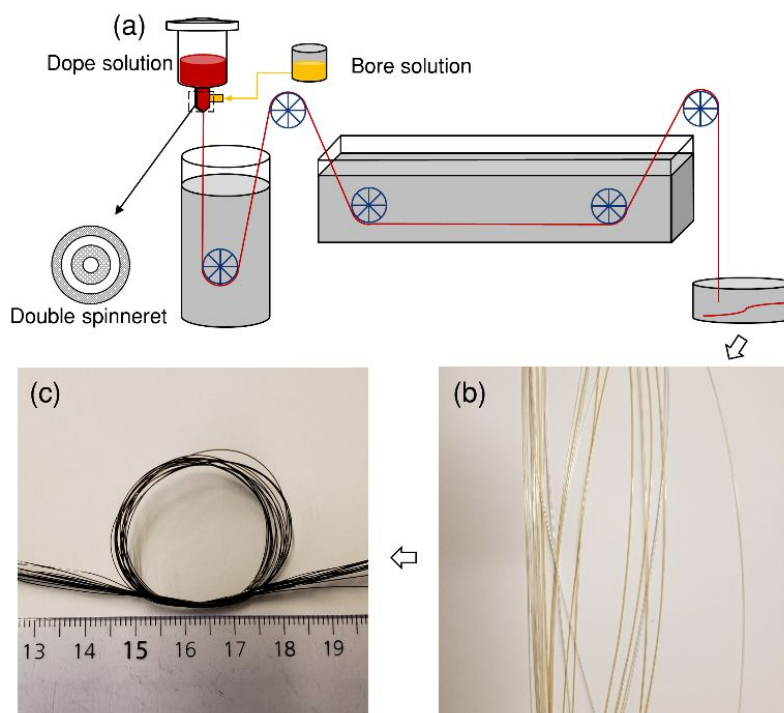

Figure 1. (a) Schematic diagram of spinning process for the cellulose hollow fiber precursors, (b) photograph of cellulose hollow fibers after washed and dried, (c) photograph of CHFMs with a remarkable flexibility

In order to investigate the influences of spinning parameters on the cellulose hollow fiber precursors and prepare high performance CHFMs, five spinning parameters; air gap, dope flow, bore composition, bore flow and take-up speed, were investigated by using a 2^{5-2} fractional factorial design method. This means 8 experiments and corresponds to a quarter of a full 2^5 design. In addition, two replicates of the center points are also performed. In total, 10 spinning batches were carried out according to the experimental design generated by Minitab 18, as listed in **Table 1**. Each factor includes high level (+1) and low level (−1). In addition, 2 center point runs are employed to estimate any inherent noise variation. The response variables

6

are the thickness, outer diameter, CO_2 permeability and CO_2/CH_4 selectivity of the prepared CHFMs carbonized at the identical conditions.

Table 1. 2^{5-2} fractional factorial design for spinning cellulose hollow fibers

Run No.	Factors				
	A	B	C	D	E
a	−1	−1	−1	+1	+1
b	+1	−1	−1	−1	−1
c	−1	+1	−1	−1	+1
d	+1	+1	−1	+1	−1
e	−1	−1	+1	+1	−1
f	+1	−1	+1	−1	+1
g	−1	+1	+1	−1	−1
h	+1	+1	+1	+1	+1
i	0	0	0	0	0
j	0	0	0	0	0

Factors	level		
	−1	+1	0
A: Air gap (mm)	10	50	30
B: Dope flow (ml/min)	2.0	4.4	3.2
C: Bore composition (water concentration, wt.%)[a]	20	30	25
D: Bore flow (ml/min)	1.1	2.4	1.8
E: Take-up speed (m/min)	7.3	14.6	11.0

[a]: the bore fluid is composed of non-solvent (water) and solvent (75 wt.% EmimAc and 25 wt.%DMSO)

7

2.3 Fabrication of carbon hollow fiber membranes

The dried cellulose hollow fibers were carbonized in a tubular furnace (Horizontal Split Tube Furnace, Carbolite Gero Limited) by applying a specific carbonization protocol, as depicted in **Figure 2**, under a CO_2 purge gas with 80 ml/min continuous flow. The protocol is chosen based on the TGA analysis of cellulose precursors and the carbonization procedure of deacetylated cellulose acetate precursors reported in the previous work [31, 39]. It should be noted that the tubular furnace was evacuated to remove other gases before being purged with CO_2. After the completion of the carbonization protocol, the system cooled down naturally and the prepared CHFMs were taken out when the temperature had cooled to below 50 °C. A typical photograph of the CHFMs is depicted in **Figure 1c**, which presents a remarkable flexibility.
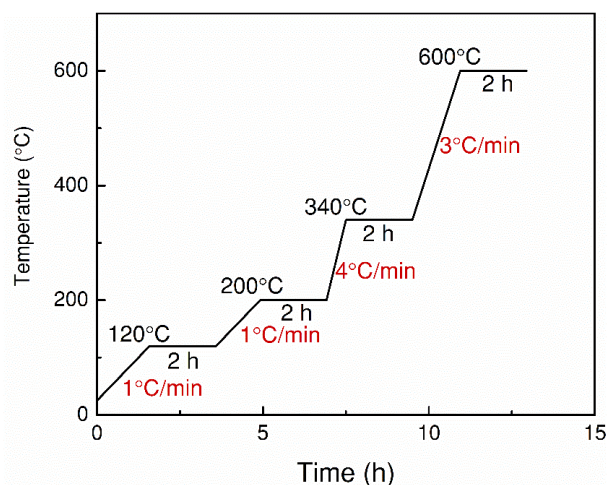

Figure 2. Carbonization protocol for cellulose hollow fiber precursors

2.4 Characterization of cellulose and carbon hollow fibers

The morphologies and structures of the precursors and carbon hollow fiber membranes were characterized by SEM (FEI Apreo and Hitachi TM3030 tabletop microscope). The cross-sectional SEM samples of cellulose hollow fiber membranes were fractured in liquid nitrogen. Pore size distribution of the CHFM sample was determined by CO_2 adsorption at 0 °C and relative pressure (P/P°) from 0.0005 to 0.031 using a TriStar II 3020 (Micromeritics Instrument Corp.). Gas sorption data were automatically analyzed by the

TriStar software using the "CO_2-DFT" model. Rubotherm magnetic suspension balance (MSB, TA Instruments) with a resolution of 1 µg was employed to obtain the density and average pore size of CHFMs by conducting helium and CO_2 adsorption with an increasing pressure from 1 bar to 20 bar with a constant flow rate of 100 ml/min at 25 ºC. The measurement procedure was described in detail elsewhere [40].

The Langmuir-Freundlich adsorption equilibrium isotherm model [40, 41] (Eq. (1)), the Dubinin-Radushkevitch (DR) equation [42] (Eq. (2)) and the Stoeckli equation [43] (Eq. (3)) were employed to evaluate the structure properties of CHFMs:

$$q = \frac{bq_m p^{1/n}}{1 + bp^{1/n}} \tag{1}$$

$$\frac{w}{w_0} = \exp\left(-\left(\frac{RTln(\frac{p_0}{p})}{\beta E_0}\right)^2\right) \tag{2}$$

$$L_0 = \frac{10.8 \ (nm \cdot kJ/mol)}{E_0 - 11.4 \ (kJ/mol)} \tag{3}$$

where q corresponds the CO_2 adsorbed amount at pressure p, b and q_m are the Langmuir affinity parameter and the maximum adsorbed amount, respectively, and n is the Langmuir-Freundlich coefficient. w and w_0 are the gas volume adsorbed at pressure p and micropore volume of CHFM, respectively. E_0 and L_0 correspond the adsorption activation energy and average micropore width of a CHFM sample. The affinity coefficient (β) used in the DR equation is 0.35 according to the literature [40]. The true density and bulk density of a sample were determined by the buoyancy experiments with the non-absorbable gas of helium [40].

2.5 Gas permeation measurements

In this work, the bore-side feeding was applied to both single gas and mixed gas permeation measurements. The single gas permeation measurements for the different batches of CHFMs were conducted on a constant permeate volume method with variable-pressure system, according to the Eq. 4,

$$P = \frac{273 \times 10^7 V \cdot r_1 ln\left(1 + \frac{l}{r_1}\right)}{76T \cdot A_{inner} \cdot \Delta P} \cdot \left(\frac{dp}{dt}\right) \tag{4}$$

9

where P (Barrer) is the pure gas permeability. V (cm³) is the downstream volume, and T (K) is the experimental temperature. l (cm) and r_1 (cm) are the thickness and inner radius of hollow fibers, respectively. A_{inner} (cm²) is the inner surface area corresponding to r_1. ΔP (bar) is the pressure drop cross the membranes. dp/dt (mbar/s) is the downstream pressure increasing rate by taking account of any small leakage in the system. In most of the literature, the permeability was calculated from the measured thickness of hollow fibers directly without considering the difference of permeate gas flux through the wall of hollow fiber caused by the radius change. The difference can be ignored if the ratio of wall thickness to radius (l/r) is very small. However, for the hollow fibers with a thick wall, the difference of gas permeability calculated based on inner and outer surface area can be significant. Thus, in this work, the term $r_1 \ln{(1 + \frac{l}{r_1})}$ in the Eq. (4) is considered as a corrected thickness using the membrane inner radius and the measured thickness. Gas permeability calculated based on the inner surface area from the Eq. (4) is identical to that of the outer surface area. The detailed derivation is described in the supporting information.

All single gas permeation tests were conducted at 25 °C with a feed pressure of 2 bar. The tests were run until a steady state had been reached implying a constant dp/dt. Two or three different membrane modules from each batch CHFM were constructed and individually tested to obtain the average gas permeabilities. The construction of membrane modules was depicted in detail by He et al. [19]. Typically, 2-4 CHFMs with an accumulative length of ~70 cm are mounted into a ¼-inch stainless steel tubing (For CHFMs with very thin wall, ~30 cm length is used due to the increased brittleness). The ideal selectivities of different gas pairs (e.g., CO_2/CH_4) are calculated as the ratio of gas permeabilities, $\alpha_{ij} = {P_i}/{P_j}$.

A relatively large size membrane module with an effective area of 9 cm² was investigated by feeding a 100 Nml/min mixed gas of 10 mol% CO_2 - 90 mol% CH_4 at varying feed pressures and temperatures. The stage-cut in all measurements was kept less than 1%. The permeation setup is illustrated in **Figure 3**. The feed gas flow and pressure are controlled by mass flow controller (MFC 1) and back pressure controller (BPC 1), respectively. The actual feed pressure was also recorded by the pressure transducers of PI1 & PI2. Sweep

10

gas (N_2) flow and pressure are controlled by MFC 2 and BPC 2, and the permeate flow including sweep

gas is measured by the mass flowmeter (MFM1, Bronkhorst, Nederland). The gas composition in the

permeate side is analyzed by a gas chromatograph (GC, 8610C, SRI Instruments Inc.). The gas temperature

in the feed, retentate and permeate side are measured by temperature indicators (TI1-3). Each experimental

point was recorded as the average of three GC samples after reaching steady state gas permeation. The

separation factor of CO_2/CH_4 is calculated by $\alpha_{CO_2/CH_4} = \frac{y_{CO_2}/y_{CH_4}}{x_{CO_2}/x_{CH_4}}$, where x_i and y_i are the concentration of

the components in the feed and permeate, respectively.
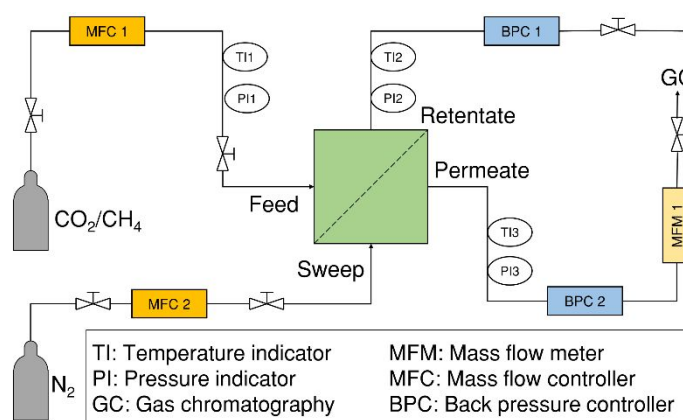

Figure 3. Illustration of the mixed gas permeation setup

2.6 Statistical analysis

Based on the obtained experimental data and characterization results, multivariate analysis was conducted

by Minitab® 18. Linear regression models for the 4 response variables were developed to fit the obtained

results according to the Eq. (5),

$$\hat{y}_i = \Sigma_{i=1}^{n} b_i x_i + b_{0,i} \tag{5}$$

where $\hat{y}_i$ is the estimated response, $b_{0,i}$ and b_i are the regression coefficient, x_i is the spinning factors and

n is the number of factors. The Pareto Charts of Standard Effects and Main Effects Plot are used to analyze

the main effects of different parameters. The Pareto Charts of Standard Effects plots the bars of absolute

values of the standardized effects from the largest to the smallest effect. If a bar exceeds a reference line,

11

the corresponding parameter is statistically significant. The standardized effects are evaluated applying t-statistics that test the null hypothesis (effect is 0), and the reference line for statistical significance is depended on the significance level α and degree of freedom (DF) of parameters. In this work, the α of 0.1 is applied for the significance level (e.g., the reference line is located at 2.132 for 5 parameters).

When the statistical significance of the main effects for each response is determined, the models will be modified by only including significant parameters. Furthermore, the statistical significance of parameters in the new model is estimated again. The percentage of variation R^2 and R^2-adj are calculated to interpret the precision of the developed models.

## 3. Results and discussion

3.1 Structure of precursor and carbon hollow fiber membranes

The dimension (thickness and diameter) of cellulose precursors among different batches are different due to different spinning conditions (listed in Table S1). **Figure 4** shows a typically cross-sectional morphology of the precursor of batch d (the SEM images of the other batches are summarized in Figure S2). Even though the composition between the bore solution (water and solvent) and the coagulation bath (tap water) are different, the cellulose hollow fibers present a symmetric structure after drying, as shown in **Figure 4c** and **4d**. This structure is very similar with the morphology of the regenerated cellulose from ILs reported in the literature [44]. In addition, extremely low permeate flow of cellulose precursors was detected by single gas permeation testing with CO_2 or helium at 5 bar, which indicated that the spun cellulose hollow fiber precursors present a dense structure.

The parameter settings according to a) and e) generated unstable spinning states (e.g., hollow fibers were easily broken during the spinning) since these settings yielded extremely thin hollow fibers with poor mechanical strength. Furthermore, the hollow fibers with thinner wall are more easily collapsed during the subsequent drying process. Additionally, the fibers with thicker walls, as revealed in **Figure S2c** and **S2g** were prone to forming a non-uniform wall. Thus, it is crucial to adjust and control the spinning parameters
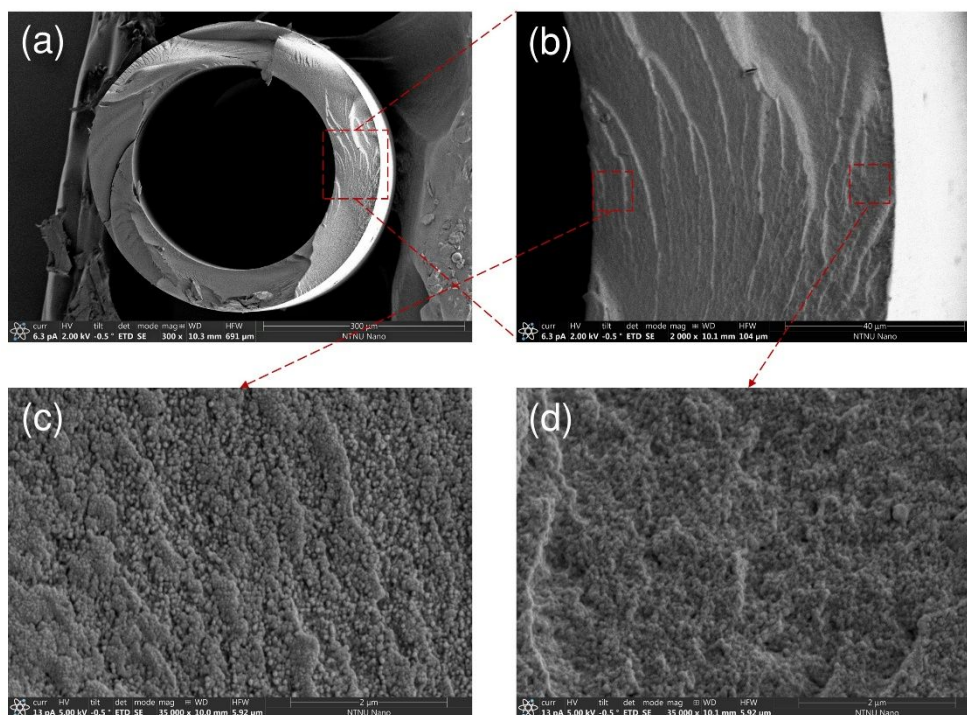
Figure 4. Cross-sectional SEM images of the (batch d) cellulose hollow fiber precursor, (c) and (d) correspond the inner and outer cross-sectional images, respectively.

Following the carbonization protocol indicated in **Figure 2**, different CHFMs were prepared from the spun cellulose hollow fiber precursors. **Figure 5** and **Figure S3** present the cross-sectional morphology of different batches CHFMs. Compared with the morphology of the cellulose precursors (batch d) in **Figure 4**, the carbonized hollow fiber membranes shown in **Figure 5** have a significant shrinkage (e.g., an average of 42 % reduction in diameter and thickness) compared to the precursors. In order to evaluate the influences of precursor structures (determined by spinning parameters) on the dimension of CHFMs, the average thickness and outer diameter of CHFMs are obtained by measuring several hollow fibers from each batch, as summarized in **Table 2**. The detailed discussion of the influences of spinning parameters on dimension of CHFMs is documented in the Appendix B of the Supporting Information.
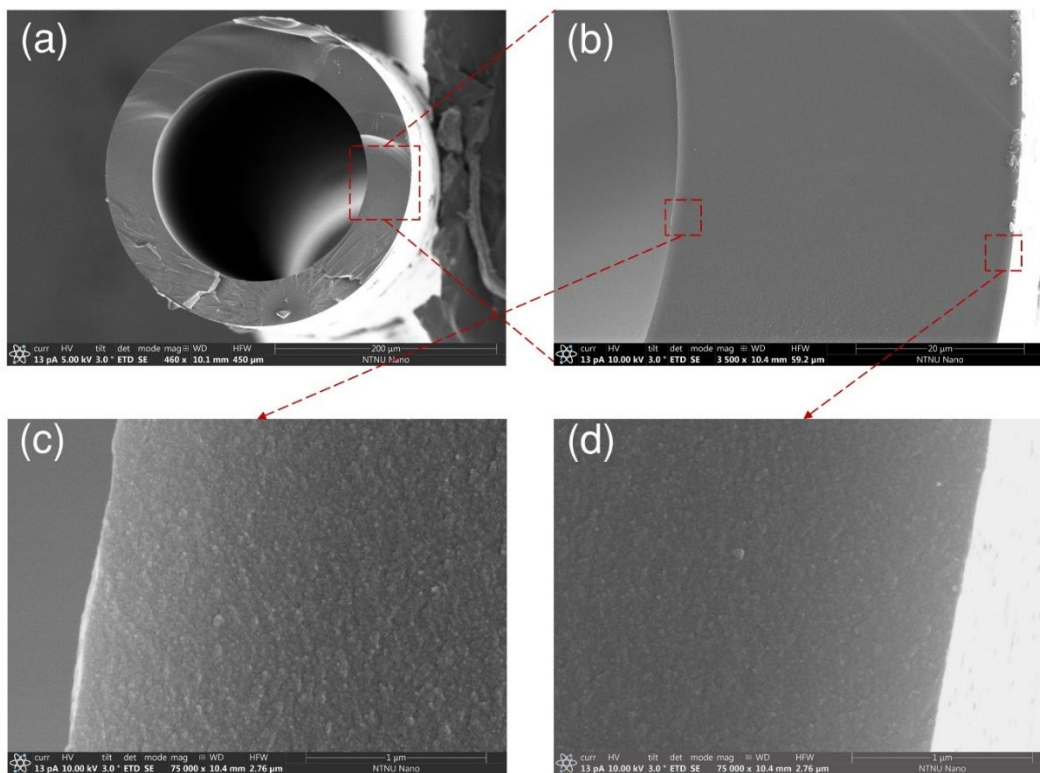
13

Figure 5. Cross-sectional SEM images of the CHFMs made from the batch d precursors

Table 2. Summary of measured responses for the CHFMs prepared by the 2^{5-2} fractional factorial design

Run No.	Measured responses			
	L, thickness (μm)	OD, outer diameter (μm)	P, CO_2 permeability (Barrer)	S, CO_2/CH_4 selectivity
a	12	224	43	59
b	22	180	171	128
c	53	200	264	173
d	46	292	239	186
e	14	237	28	69
f	21	162	122	123
g	55	250	86	321
h	35	240	188	112
i	31	211	124	116
j	30	208	133	128

14

3.2 Single gas permeation properties of carbon hollow fiber membranes

The gas permeabilities of different batch CHFMs based on single gas permeation testing are plotted in

Figure 6 as a function of the gas kinetic diameter [45]. The gas permeation through the CHFMs is mainly

dependent on the kinetic diameters of gas molecules, which implies the transport mechanism is molecular

sieving dominated. By changing the spinning parameters, the CO_2 permeability ranges from 28 Barrer

(batch e) to 264 Barrer (batch c). This indicates that some of the spinning parameters can influence the gas

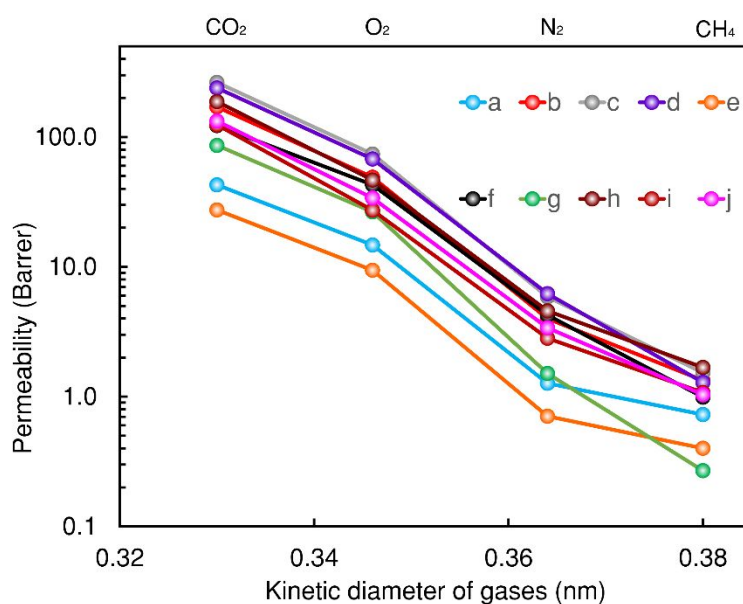permeation performances of the obtained CHFMs significantly.

Figure 6. Single-gas permeabilities through different batches CHFMs as a function of gas kinetic

diameter at 25 °C and 2 bar

Figure 7 illustrates the Robeson upper bound of CO_2/CH_4 and O_2/N_2 separation performances obtained in

this work and comparisons with some CMS membranes produced from cellulosic precursors reported in

the literature [19, 26, 46]. By adjusting the spinning parameters, most of prepared CHFMs show good permeation

performances that are above the Robeson upper bound of CO_2/CH_4. Besides, all of them exceed O_2/N_2

upper bound. Compared with flat sheet CMS membranes reported by Lie and Hägg [46], the fabricated

CHFMs show higher selectivity for CO_2/CH_4 and O_2/N_2. Approximately 20 times higher CO_2 permeability

than the latest flat sheet CMS membranes prepared from cellulose/ionic liquid reported by Rodrigues et al.

15

[26] has been obtained in this work. The influence on separation performance caused by spinning parameters is discussed in section 3.3. Considering the industrial applications of CO_2 removal from natural gas, high gas permeance is preferred for membranes with a thin selective layer. Therefore, making asymmetric carbon membranes from cellulose precursors should be conducted in the future work.
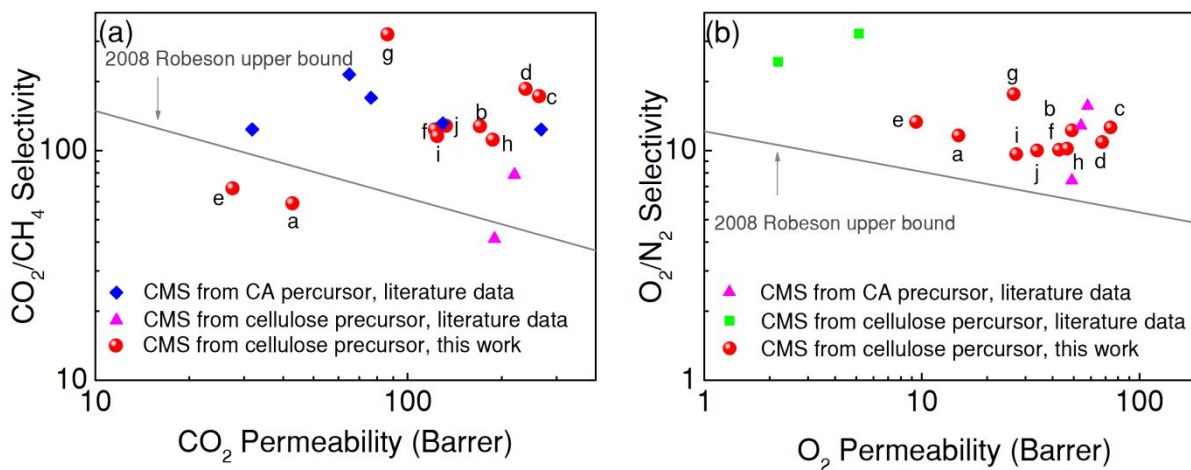

Figure 7. Separation performances of (a) CO_2/CH_4, (b) O_2/N_2 (red spheres represent the permeation data reported in this work, blue diamonds are the literature data of CMS membranes derived from cellulose acetate (CA) [19], pink triangles are literature data of CMS membranes derived from cellulose [46], green squares are literature data of CMS membranes derived from cellulose [26], the lines are the 2008 Robeson upper bound of CO_2/CH_4 and O_2/N_2, respectively [7].)

3.3 Influences of spinning parameters on performances of carbon hollow fiber membranes

Based on the single gas permeation testing results listed in **Table 2**, the linear regression models of the CO_2 permeability and CO_2/CH_4 selectivity including five factors are obtained and presented in the Eqs. (6) and (7), respectively. The non-significant factors, corresponding to the smaller regression coefficients (i.e., the smaller Pareto Chart of Standardized Effects than the reference lines as shown in **Figures S4c** and **S4d**), are taken out in the modified models of the Eqs. (8) and (9). It should be noted that the significance of take-up speed (factor E) does not exceed the reference line in the standardized effects Pareto chart for the CO_2/CH_4 selectivity (see **Figure S4d**). It is, however, still included in the statistically significant model

(Eq. (9)) since the effect is much more profound than air gap (factor A) and bore composition (factor C) (see Eq. (7)).

$$P_0 = 139.7 + 37.4A + 51.7B - 36.6C - 18.3D + 11.6E \tag{6}$$

$$S_0 = 141.3 - 9.0A + 51.5B + 10.0C - 40.0D - 29.5E \tag{7}$$

$$P_1 = 139.7 + 37.4A + 51.7B - 36.6C \tag{8}$$

$$S_1 = 141.3 + 51.5B - 40.0D - 29.5E \tag{9}$$

The Pareto Chart of Standardized Effects (**Figures 8a**) and the Main Effects Plot (**Figures** S6c) indicate that the CO_2 permeability is significantly affected by the air gap (factor A) and dope flow (factor B) in a positive trend but drops with the increase of water content in the bore composition (factor C). The CO_2/CH_4 selectivity is favored by the increase of dope flow (factor B), while bore flow (factor D) and take-up speed have negative significant effects on the CO_2/CH_4 selectivity. According to the analysis of variance for CO_2 permeability and CO_2/CH_4 selectivity, listed in **Table S2**, the P-values are much smaller than the significant level ($\alpha = 0.1$), illustrating that the models are reliable.
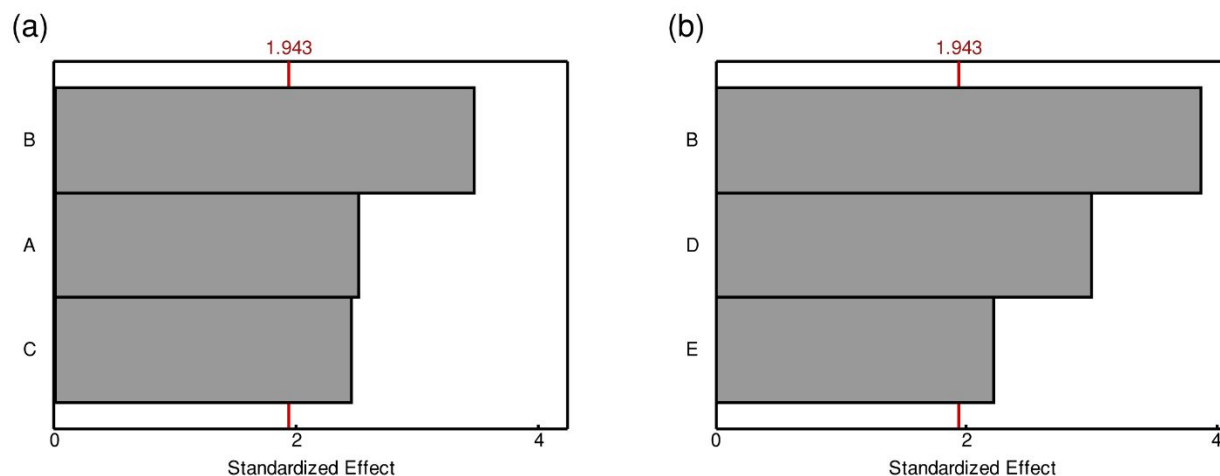
Figure 8. Pareto Chart of Standardized Effects on (a) CO_2 permeability, and (b) CO_2/CH_4 selectivity.

In this work, based on the fact that carbonization protocol is identical for the different spinning batches, the influence of carbonization on the structure changes is supposed to equal level (which is included as a constant in the developed models). Thus, the CHFMs performance is significantly dependent on precursor

17

structures. The change of bore flow rate and air gap will lead to the formation of different precursor's structure during spinning and cellulose regenerated process even though this is not evident from SEM pictures. Normally, the increase of dope flow rate, leading to a higher shear stress of dope, produces a stronger molecular chain orientation of hollow fiber during the spinning [47, 48]. Meanwhile, a bigger air gap may increase the stress parallel to the fiber axis because of a stronger gravitational influence, resulting a molecular orientation as well. Therefore, both the increase of bore flow rate and air gap could improve the permeability.

Bore fluid composition inducing morphological change in hollow fiber membranes has been presented in literature with conflicting observations. For instance, Dong et al. reported that the fraction of macrovoids in the hollow fiber wall were reduced gradually and defect-free hollow fibers were obtained afterwards by decreasing water content in the bore fluid[49]. However, formation of a macrovoid-free membrane structure by increasing water content in the bore fluid was reported by Chang et. al[50]. In this work, even though the bore composition presents a nonsignificant effect on the morphology of the fabricated CHFMs from SEM images, it exhibits a significant negative effect on the gas permeability of the CHFMs as indicated in Eq. (8). It is suggested that employing a strong non-solvent (like water) in the bore fluid would form a smooth and dense surface while a weak non-solvent bore fluid (DMSO) would lead to a relatively rough and porous surface [51]. Therefore, the carbon membranes made from the precursors spun with a higher water content bore fluid (e.g., batch g) probably form a denser inner layer, which increases the transport resistance of gas molecules, and thus presented a lower permeability compared the batch c (i.e., the precursors spun with a lower water content bore fluid).

Overall, the linear models (with $R^2 > 0.8$ and R^2-adj > 0.7) developed for CO_2 permeability and CO_2/CH_4 selectivity (Eqs. (8) and (9)) can be employed to preliminary predict the separation performances of CHFMs before spinning. Moreover, the developed linear models for thickness and diameter (see Eqs. (S9) and (S10) in the Supporting Information) can be preliminary used to predict the dimensions of CHFMs before spinning of cellulose precursors without considering a complex mass transfer behavior during cellulose

18

regeneration process. The optimal spinning condition for making best carbon membranes within the investigated levels is found to be (A B C D E, + + - - -) based on the Eqs. (8) and (9). The batch d is based on the precursor obtained under the spinning condition that is very close to the optimal one, and thus selected for further characterization.

3.4 Structure properties of carbon hollow fiber membranes

Considering the carbon membranes made from the precursors of the batch d presenting a good pure gas performance with CO_2 permeability of 239 Barrer and CO_2/CH_4 selectivity of 186 and uniform thickness wall, CO_2 sorption measurements were also run to characterize the structure properties. The pore size distribution of the CHFM of the batch d presents a typical bimodal distribution of ultramicropores (4.5– 7 Å) and supermicropores (7–10 Å) based on gas sorption measurement, as shown in **Figure 9a**. This bimodal pore size distribution provides a good support of good permeation performance where the ultramicropores are responsible for the high selectivity while the micropores are responsible for gas permeability. Besides, the higher-pressure CO_2 adsorption equilibrium isotherm at 25 °C (**Figure 9b**) and the corresponding Dubinin-Radushkevitch (DR) equation fitting model (**Figure 9c**) are summarized in **Table 3**. As shown in **Figure 9b**, the adsorption data are well fitted with the Langmuir- Freundlich model. The true density and bulk density of the CHFM are obtained from the buoyancy test with the non-absorbable helium. As shown in **Figure 9d**, it presents a well-fitting between the gas density and the total weight of the MSB balance. The prepared CHFM in this work presents an average micropore width of 5.9 Å and a lower bulk density of 1.1 g/cm^3, which is similar to the other regenerated cellulose based carbon membranes reported in the literature [40, 52].

Table 3. Summary of structural characteristics of CHFM

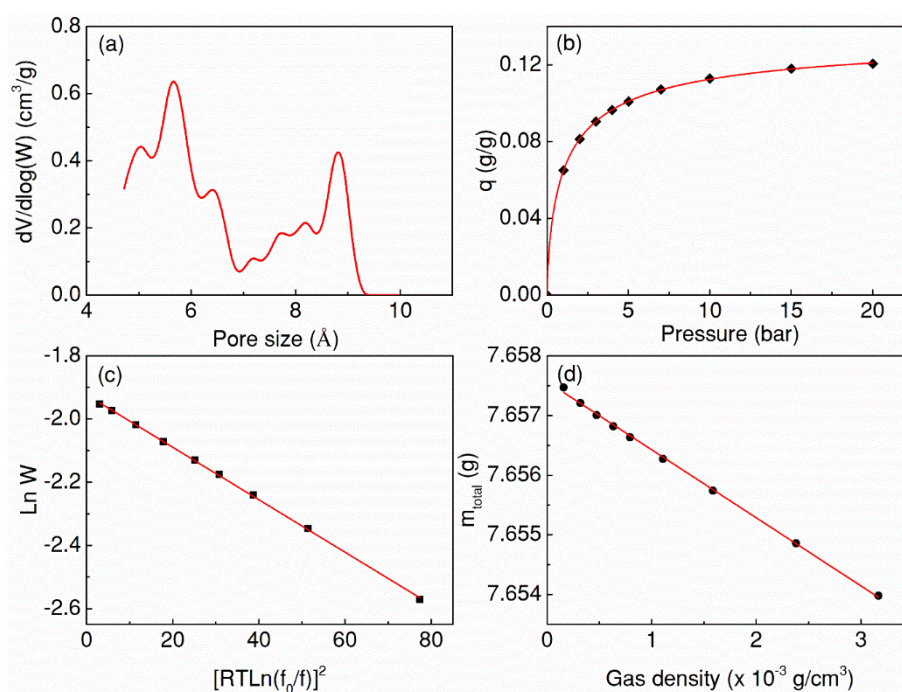| CMS membranes	Langmuir-Freundlich model			DR model		Average micropore width, L_0 (Å)	Bulk density (g/cm^3)
	b (bar^{-1})	q_m (g/g)	n	w_0 (cm^3/g)	E_0 (kJ/mol)		
This work	0.89	0.14	1.41	0.15	31.4	5.9	1.1
HFCM-1[40]	0.73	0.17	1.65	0.15	32.2	5.2	1.24
CMSM2[52]	0.93	0.15	1.34	0.16	35.6	4.5	1.3

Figure 9. Structure characterization of batch d CHFM, a) pore size distribution between 4.5-10 Å characterized at 0 ℃, b) Equilibrium CO_2 isotherm adsorption at 25 ℃ with a constant flow rate of 100 Nml/min, solid line corresponds to the Langmuir-Freundlich fitting model, c) DR fitting model according

to CO_2 adsorption, d) Helium Buoyancy measurement at 25 °C with a constant flow rate of 100 Nml/min, solid line corresponds the linear regression.

3.5 CO_2/CH_4 mixed gas permeation performance

As shown in **Figure 10**, the prepared carbon membrane demonstrates good CO_2/CH_4 separation performance at various feed pressure. The CH_4 permeability is almost constant when increasing feed pressure, while the CO_2 permeability slightly decreases, resulting in an apparent reduction of CO_2/CH_4 separation factor with the raise of the total feed pressure. It is suggested that the apparent reduction in selectivity with the increase of feed pressure can be explained via a competitive effect for sorption sites by CH_4 and gas-phase non-idealities at high pressures could decrease the CO_2 permeability [53, 54]. The competitive sorption for Langmuir sorption sites increases more significant as CH_4 has a much higher concentration and thus "outcompetes" the sorption sites of CO_2 when increasing the feed pressure [54]. As a result, the CO_2 permeability and CO_2/CH_4 separation factor decrease with the increase of feed pressure.
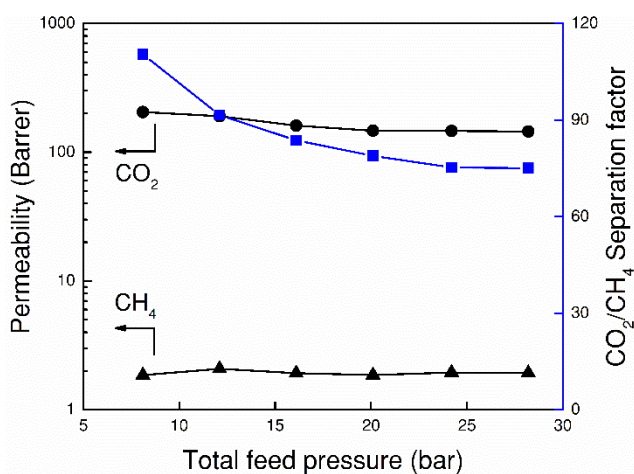

Figure 10. CO_2 permeability and CO_2/CH_4 separation factor of batch d) CHFM under different feed pressures at 25 °C

Figure 11 illustrates the temperature dependence of separation performance operated at a feed pressure of 8 bar. By increasing the operation temperatures from 25 to 60 °C, both CO_2 and CH_4 permeabilities increase whereas the separation factor decreases. Increasing operating temperature enhances the CO_2 diffusion

21

coefficient, but the CO_2 adsorption in the carbon matrix decreases. Overall, it causes a relatively slower

increase of CO_2 permeability compared to that of CH_4. The apparent transport activation energies,

calculated by linear regression of ln (P) and $1/T$ based on the Arrhenius equation ($P = P_0 e^{-\frac{E_a}{RT}}$), are 6.7

and 25.4 kJ/mol for CO_2 and CH_4, respectively. Since the transport activation energies indicate a probability

of a molecular passing through the membrane barrier, the larger E_a of CH_4 indicates a lower permeability

at the same operating temperature but a more significant effect of temperature. Despite the separation factor

decreases with the increase of operating temperature, the carbon membrane still maintains an attractive

separation factor of 50 at 60 ℃. Thus, moderate temperature is probably preferred for CHFMs to achieve a

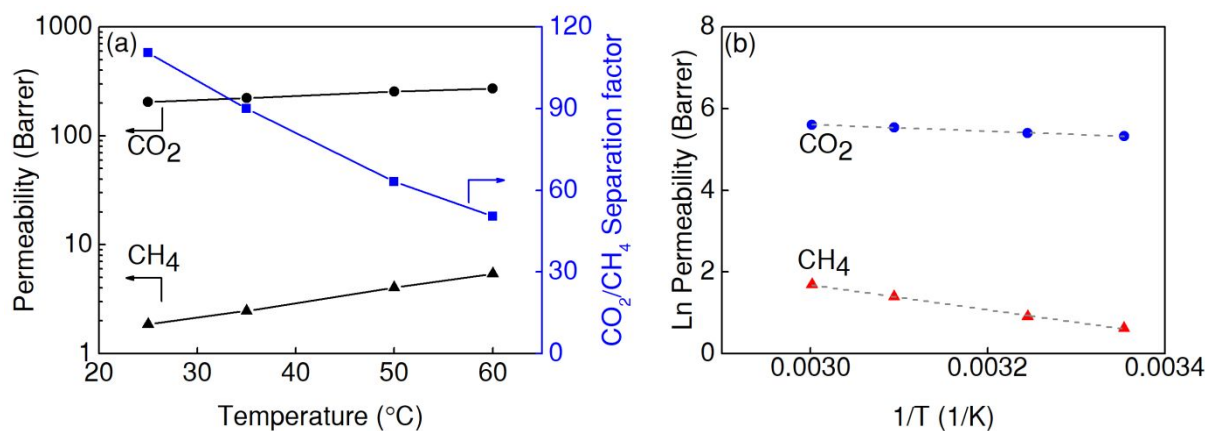high gas permeability without a significant loss of separation factor.

Figure 11. Effects of operation temperature (25 to 60 ℃) on separation performance of batch d CHFM

(feed pressure is 8 bar). (a) Temperature dependence of CO_2 permeability and CO_2/CH_4 separation factor;

(b) Arrhenius plots according to CO_2 and CH_4 permeability

4. Conclusions

In this work, novel CHFMs are prepared based on the cellulose hollow fiber precursors spun from the

cellulose-EmimAc/DMSO solutions. The effects of spinning parameters on the dimensions and separation

performances of the prepared CHFMs are systematically investigated by the multivariate analysis of the

results from the 2^{5-2} fractional factorial design. The regression models reveal that thickness and diameter of

22

CHFMs are mainly determined by the spinning parameters of dope flow rate, bore flow rate and take-up speed. The models of CO_2 permeability and CO_2/CH_4 selectivity imply that the separation performances of CHFMs are influenced by precursor structures obtained under different spinning parameters. In addition, the 2008 Robeson upper bound is surpassed for CO_2/CH_4 separation, and all CHFMs for O_2/N_2 separation. Moreover, the prepared CHFM presents a micropore volume of 0.15 cm^3/g and an average pore size of 5.9 Å, which provide a higher separation performance with CO_2 permeability of 239 Barrer and CO_2/CH_4 selectivity 186. The mixture testing of 10% CO_2 - 90% CH_4 operated at different pressures and temperatures revealed that the obtained CHFM shows an attractive selectivity of 75 at 28 bar feed pressure. Increasing operating temperature slightly decreases the CO_2/CH_4 selectivity due to a faster increment of CH_4 permeability than CO_2, CO_2 permeability remained constant. Overall, the developed novel CHFMs from cellulose precursors present a potential application in high-pressure natural gas sweetening or other gas separation processes.

Acknowledgement

Author information

Corresponding Authors

Prof. Magne Hillestad, Email: magne.hillestad@ntnu.no (MH)

Dr. Xuezhong He, xuezhong.he@ntnu.no (XH), Tel.: +47-7359-3942

Conflicts of interest

23

The authors declare no conflict of interest.

Supporting Information

Appendix A. Calculation of the permeability of carbon hollow fiber membrane (CHFM)

Appendix B. Influences of spinning parameters on dimension of carbon hollow fiber membranes

Figure S1. Schematic diagram of a cross-sectional CHFM

Figure S2. Cross-sectional SEM images of spun cellulose hollow fibers from batch a to j following the 2^{5-2} fractional factorial design

Figure S3. Cross-sectional SEM images of the 10 batches (from a to j) CHFMs made from cellulose hollow fiber precursors

Figure S4. Pareto Chart of Standardized Effects on a) thickness, b) outer diameter, c) CO_2 permeability, and d) CO_2/CH_4 selectivity in the original models

Figure S5. Pareto Chart of Standardized Effects on (a) thickness, (b) outer diameter in the improved models

Figure S6. The main effects of spinning parameters on a) thickness, b) outer diameter, c) CO_2 permeability, and d) CO_2/CH_4 selectivity

Table S1. Summary of the dimension of cellulose hollow fiber membranes

Table S2. Analysis of variance for 4 improved linear models

References

1.   Badwal, S. P. S.; Ciacchi, F. T. Ceramic Membrane Technologies for Oxygen Separation. *Advanced Materials* **2001,** 13, (12-13), 993-996.
2.   Baker, R. W.; Lokhandwala, K. Natural Gas Processing with Membranes: An Overview. *Industrial & Engineering Chemistry Research* **2008,** 47, (7), 2109-2121.
3.   Liu, G.; Li, N.; Miller, S. J.; Kim, D.; Yi, S.; Labreche, Y.; Koros, W. J. Molecularly Designed Stabilized Asymmetric Hollow Fiber Membranes for Aggressive Natural Gas Separation. *Angewandte Chemie* **2016,** 128, (44), 13958-13962.

24

4.   Belmabkhout, Y.; Bhatt, P. M.; Adil, K.; Pillai, R. S.; Cadiau, A.; Shkurenko, A.; Maurin, G.; Liu, G.; Koros, W. J.; Eddaoudi, M. Natural gas upgrading using a fluorinated MOF with tuned H2S and CO2 adsorption selectivity. *Nature Energy* **2018,** 3, (12), 1059-1066.

5.   He, X.; Hägg, M.-B. Hollow fiber carbon membranes: Investigations for CO_2 capture. *J Membr Sci* **2011,** 378, (1-2), 1-9.

6.   Liu, L.; Chakma, A.; Feng, X. Preparation of hollow fiber poly(ether block amide)/polysulfone composite membranes for separation of carbon dioxide from nitrogen. *Chemical Engineering Journal* **2004,** 105, (1), 43-51.

7.   Robeson, L. M. The upper bound revisited. *J Membr Sci* **2008,** 320, (1-2), 390-400.

8.   Adams, J. S.; Itta, A. K.; Zhang, C.; Wenz, G. B.; Sanyal, O.; Koros, W. J. New insights into structural evolution in carbon molecular sieve membranes during pyrolysis. *Carbon* **2019,** 141, 238-246.

9.   Favvas, E. P.; Romanos, G. E.; Katsaros, F. K.; Stefanopoulos, K. L.; Papageorgiou, S. K.; Mitropoulos, A. C.; Kanellopoulos, N. K. Gas permeance properties of asymmetric carbon hollow fiber membranes at high feed pressures. *Journal of Natural Gas Science and Engineering* **2016,** 31, 842-851.

10.   Zhang, C.; Koros, W. J. Ultraselective Carbon Molecular Sieve Membranes with Tailored Synergistic Sorption Selective Properties. *Advanced Materials* **2017,** 29, (33), 1701631.

11.   He, X.; Hägg, M.-B. Hollow fiber carbon membranes: From material to application. *Chemical Engineering Journal* **2013,** 215-216, 440-448.

12.   Yang, X.; Li, Z.; Zhang, C.; Wang, H.; Zhang, E.; Xing, Y.; Xiao, P.; Yang, R. T.; Liu, Y.; Webley, P. A. Practical separation performance evaluation of coal mine methane upgrading with carbon molecular sieves. *Chemical Engineering Journal* **2019,** 367, 295-303.

13.   Zhang, P.; Zhong, Y.; Ding, J.; Wang, J.; Xu, M.; Deng, Q.; Zeng, Z.; Deng, S. A new choice of polymer precursor for solvent-free method: Preparation of N-enriched porous carbons for highly selective CO_2 capture. *Chemical Engineering Journal* **2019,** 355, 963-973.

14.   Agarwal, K.; John, M.; Pai, S.; Newalkar, B. L.; Bhargava, R.; Choudary, N. V. SAPO-34 assisted C3 separation: Modeling and simulation. *Microporous and Mesoporous Materials* **2010,** 132, (3), 311-318.

15.   Chew, T. L.; Ahmad, A. L.; Bhatia, S. Ba-SAPO-34 membrane synthesized from microwave heating and its performance for CO_2/CH_4 gas separation. *Chemical Engineering Journal* **2011,** 171, (3), 1053-1059.

16.   Favvas, E. P.; Romanos, G. E.; Papageorgiou, S. K.; Katsaros, F. K.; Mitropoulos, A. C.; Kanellopoulos, N. K. A methodology for the morphological and physicochemical characterisation of asymmetric carbon hollow fiber membranes. *Journal of Membrane Science* **2011,** 375, (1), 113-123.

17.   Ning, X.; Koros, W. J. Carbon molecular sieve membranes derived from Matrimid® polyimide for nitrogen/methane separation. *Carbon* **2014,** 66, 511-522.

18.   He, X.; Hagg, M.-B. Optimization of Carbonization Process for Preparation of High Performance Hollow Fiber Carbon Membranes. *Ind Eng Chem Res* **2011,** 50, (13), 8065-8072.

19.   He, X.; Lie, J. A.; Sheridan, E.; Hagg, M.-B. Preparation and Characterization of Hollow Fiber Carbon Membranes from Cellulose Acetate Precursors. *Ind Eng Chem Res* **2011,** 50, (4), 2080-2087.

20.   He, X.; Kim, T.-J.; Hägg, M.-B. Hybrid fixed-site-carrier membranes for CO_2 removal from high pressure natural gas: Membrane optimization and process condition investigation. *J Membr Sci* **2014,** 470, (0), 266-274.

21.   Haider, S.; Lie, J.; Lindbråthen, A.; Hägg, M.-B. J. M. Pilot–Scale Production of Carbon Hollow Fiber Membranes from Regenerated Cellulose Precursor-Part I: Optimal Conditions for Precursor Preparation. *Membranes* **2018,** 8, (4), 105.

22.   Klemm, D.; Heublein, B.; Fink, H.-P.; Bohn, A. Cellulose: Fascinating Biopolymer and Sustainable Raw Material. *Angewandte Chemie International Edition* **2005,** 44, (22), 3358-3393.

25

23.   Wang, H.; Gurau, G.; Rogers, R. D. Ionic liquid processing of cellulose. *Chemical Society Reviews* **2012,** 41, (4), 1519-1537.

24.   Park, C. H.; Jeon, S.; Park, S.-H.; Shin, M. G.; Park, M. S.; Lee, S.-Y.; Lee, J.-H. Cellulose nanocrystal-assembled reverse osmosis membranes with high rejection performance and excellent antifouling. *Journal of Materials Chemistry A* **2019,** 7, (8), 3992-4001.

25.   Puspasari, T.; Chakrabarty, T.; Genduso, G.; Peinemann, K.-V. Unique cellulose/polydimethylsiloxane blends as an advanced hybrid material for organic solvent nanofiltration and pervaporation membranes. *Journal of Materials Chemistry A* **2018,** 6, (28), 13685-13695.

26.   Rodrigues, S. C.; Andrade, M.; Moffat, J.; Magalhães, F. D.; Mendes, A. Preparation of carbon molecular sieve membranes from an optimized ionic liquid-regenerated cellulose precursor. *Journal of Membrane Science* **2019,** 572, 390-400.

27.   Zhu, S.; Wu, Y.; Chen, Q.; Yu, Z.; Wang, C.; Jin, S.; Ding, Y.; Wu, G. Dissolution of cellulose with ionic liquids and its application: a mini-review. *Green Chemistry* **2006,** 8, (4), 325-327.

28.   Liu, Y.; Meyer, A. S.; Nie, Y.; Zhang, S.; Thomsen, K. Low energy recycling of ionic liquids via freeze crystallization during cellulose spinning. *Green Chemistry* **2018,** 20, (2), 493-501.

29.   Lynam, J. G.; Chow, G. I.; Coronella, C. J.; Hiibel, S. R. Ionic liquid and water separation by membrane distillation. *Chemical Engineering Journal* **2016,** 288, 557-561.

30.   Liu, X.; Nie, Y.; Meng, X.; Zhang, Z.; Zhang, X.; Zhang, S. DBN-based ionic liquids with high capability for the dissolution of wool keratin. *RSC Advances* **2017,** 7, (4), 1981-1988.

31.   Lei, L.; Lindbråthen, A.; Sandru, M.; Gutierrez, M.; Zhang, X.; Hillestad, M.; He, X. Spinning Cellulose Hollow Fibers Using 1-Ethyl-3-methylimidazolium Acetate–Dimethylsulfoxide Co-Solvent. *Polymers* **2018,** 10, (9), 972.

32.   Khayet, M.; Seman, M. N. A.; Hilal, N. Response surface modeling and optimization of composite nanofiltration modified membranes. *Journal of Membrane Science* **2010,** 349, (1), 113-122.

33.   Xiangli, F.; Wei, W.; Chen, Y.; Jin, W.; Xu, N. Optimization of preparation conditions for polydimethylsiloxane (PDMS)/ceramic composite pervaporation membranes using response surface methodology. *Journal of Membrane Science* **2008,** 311, (1), 23-33.

34.   Khayet, M.; Cojocaru, C.; García-Payo, M. C. Experimental design and optimization of asymmetric flat-sheet membranes prepared for direct contact membrane distillation. *Journal of Membrane Science* **2010,** 351, (1), 234-245.

35.   Saljoughi, E.; Sadrzadeh, M.; Mohammadi, T. Effect of preparation variables on morphology and pure water permeation flux through asymmetric cellulose acetate membranes. *Journal of Membrane Science* **2009,** 326, (2), 627-634.

36.   Barber, P. S.; Griggs, C. S.; Gurau, G.; Liu, Z.; Li, S.; Li, Z.; Lu, X.; Zhang, S.; Rogers, R. D. Coagulation of Chitin and Cellulose from 1-Ethyl-3-methylimidazolium Acetate Ionic-Liquid Solutions Using Carbon Dioxide. *Angewandte Chemie International Edition* **2013,** 52, (47), 12350-12353.

37.   Wang, R.; Shi, L.; Tang, C. Y.; Chou, S.; Qiu, C.; Fane, A. G. Characterization of novel forward osmosis hollow fiber membranes. *Journal of Membrane Science* **2010,** 355, (1), 158-167.

38.   Ren, J.; McCutcheon, J. R. Polyacrylonitrile supported thin film composite hollow fiber membranes for forward osmosis. *Desalination* **2015,** 372, 67-74.

39.   He, X. Development of Hollow Fiber Carbon Membranes for CO_2 Separation. PhD, Norwegian University of Science and Technology, Trondheim, 2011.

40.   He, X.; Hägg, M.-B. Structural, kinetic and performance characterization of hollow fiber carbon membranes. *Journal of Membrane Science* **2012,** 390-391, 23-31.

41.   Yu, J. W.; Neretnieks, I. Single-component and multicomponent adsorption equilibria on activated carbon of methylcyclohexane, toluene, and isobutyl methyl ketone. *Industrial & Engineering Chemistry Research* **1990,** 29, (2), 220-231.

26

42.   Dubinin, M. M. Generalization of the theory of volume filling of micropores to nonhomogeneous microporous structures. *Carbon* **1985,** 23, (4), 373-380.

43.   Stoeckli, F.; Slasli, A.; Hugi-Cleary, D.; Guillot, A. The characterization of microporosity in carbons with molecular sieve effects. *Microporous and Mesoporous Materials* **2002,** 51, (3), 197-202.

44.   Sukma, F. M.; Çulfaz-Emecen, P. Z. Cellulose membranes for organic solvent nanofiltration. *J Membr Sci* **2018,** 545, 329-336.

45.   Mulder, J. *Basic principles of membrane technology*. Springer Science & Business Media: 2012.

46.   Lie, J. A.; Hagg, M.-B. Carbon membranes from cellulose: Synthesis, performance and regeneration. *J Membr Sci* **2006,** 284, (1-2), 79-86.

47.   Chung, T.-S.; Lin, W.-H.; Vora, R. H. The effect of shear rates on gas separation performance of 6FDA-durene polyimide hollow fibers. *Journal of Membrane Science* **2000,** 167, (1), 55-66.

48.   Ismail, A. F.; Dunkin, I. R.; Gallivan, S. L.; Shilton, S. J. Production of super selective polysulfone hollow fiber membranes for gas separation. *Polymer* **1999,** 40, (23), 6499-6506.

49.   Dong, G.; Li, H.; Chen, V. Factors affect defect-free Matrimid® hollow fiber gas separation performance in natural gas purification. *Journal of Membrane Science* **2010,** 353, (1), 17-27.

50.   Chang, J.; Zuo, J.; Zhang, L.; O'Brien, G. S.; Chung, T.-S. Using green solvent, triethyl phosphate (TEP), to fabricate highly porous PVDF hollow fiber membranes for membrane distillation. *Journal of Membrane Science* **2017,** 539, 295-304.

51.   Ahmad, A. L.; Otitoju, T. A.; Ooi, B. S. Hollow fiber (HF) membrane fabrication: A review on the effects of solution spinning conditions on morphology and performance. *Journal of Industrial and Engineering Chemistry* **2019,** 70, 35-50.

52.   Lagorsse, S.; Magalhães, F. D.; Mendes, A. Carbon molecular sieve membranes: Sorption, kinetic and structural characterization. *J Membr Sci* **2004,** 241, (2), 275-287.

53.   Swaidan, R.; Ma, X.; Litwiller, E.; Pinnau, I. High pressure pure- and mixed-gas separation of CO2/CH4 by thermally-rearranged and carbon molecular sieve membranes derived from a polyimide of intrinsic microporosity. *Journal of Membrane Science* **2013,** 447, 387-394.

54.   Vu, D. Q.; Koros, W. J.; Miller, S. J. High Pressure CO_2/CH_4 Separation Using Carbon Molecular Sieve Hollow Fiber Membranes. *Ind Eng Chem Res* **2002,** 41, (3), 367-380.

27

1
2
3
4
5
6
7
8
9
10
11
12
13
14
15
16
17
18
19
20
21
22
23
24
25
26
27
28
29
30
31
32
33
34
35
36
37
38
39
40
41
42
43
44
45
46
47
48
49
50
51
52
53
54
55
56
57
58
59
60

For Table of Contents Only